NJC

New Journal of Chemistry

A journal for new directions in chemistry

Accepted Manuscript

This article can be cited before page numbers have been issued, to do this please use: J. Bore, S.M. A. Rafat, C. Hoffert, A. Ellis, C. Blake, C. Celis-Barros, W. Chen, A. Boika, B. Schrage and C. Ziegler, *New J. Chem.*, 2026, DOI: 10.1039/D6NJ01601D.

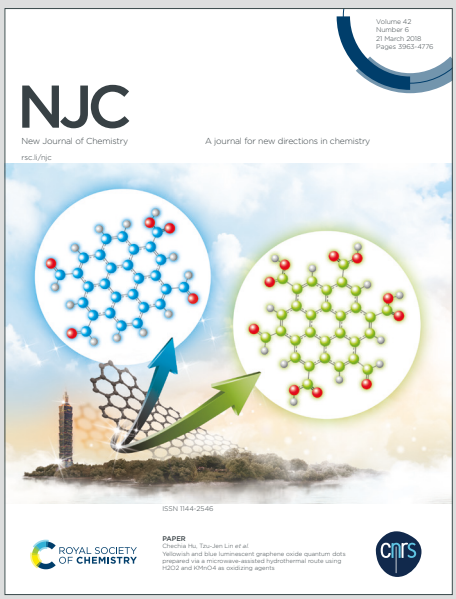

View Article Online
DOI: 10.1039/D6NJ01601D

ARTICLE

The High-Valent Vanadium Chemistry of Isoindoline Chelates

Joan C. Bore,[a] S. M. Al Rafat,[a] Clara A. Hoffert,[a] Allison A. Ellis,[a] Cameron Blake,[a] Cristian Celis-Barros,[b] Wei-Yuan Chen,[a] Aliaksei Boika,[a] Briana R. Schrage,*[b] and Christopher J. Ziegler*[a]

prReceived 00th January 20xx,
Accepted 00th January 20xx

DOI: 10.1039/x0xx00000x

Isoindoline-based chelates have shown extensive metal binding chemistry—in particular, bis(arylimino)isoindolines. Although this chemistry has been explored for the middle and late transition metal ions, little work has been carried out on early transition metal complexes. In this article, we present the first examples of vanadium coordinated using four bis(arylimino)isoindolines, in which the aryl groups are pyrazole, indazole, benzimidazole, and pyridine (ligands **1–4**, respectively). We isolated five complexes using vanadyl sulfate or vanadyl acetylacetonate as the vanadium source. In all cases, the ligands bound in a meridional mode, and for four of the complexes, the vanadium ion was observed in the V(V) oxidation state. Three of the ligands (**1–3**) formed VO_2 complexes with vanadyl sulfate and vanadyl acetylacetonate, but the bis(pyridylimino)isoindoline (ligand **4**) formed a V(V) oxosulfonato complex with the former starting material and a vanadyl V(IV) acetylacetonate with the latter starting material. All metal compounds were structurally elucidated by X-ray crystallographic methods, and we probed their electronic structures using DFT methods.

Introduction

The chemistry of vanadium compounds remains an important area of fundamental scientific investigation. Researchers continue to pursue the basic coordination chemistry of vanadium. Vanadium is a versatile early transition metal and can readily access several oxidation states, V(II), V(III), V(IV), and V(V). Vanadium in the +5 oxidation state is often used as catalysts and can be used to mediate organic transformations. For example, V(V) oxide is commonly employed as a catalyst in the production of sulfuric acid.[1] Additionally, vanadium(V) complexes serve as catalysts for substrate oxidations or olefin polymerization reactions.[2–6] Furthermore, vanadium centers play roles in bioinorganic chemistry, such as in the metal cluster cofactor of vanadium nitrogenase,[7,8] the active site in vanadium bromoperoxidase,[9–11] or the fungal natural product amavadin.[7,12,13]

This metal has also been employed for energy storage applications, specifically as the most well-known and well-studied single-component redox flow battery material.[14–18] The vanadium redox flow battery utilizes vanadium's ability to exist in four oxidation states, with V(II)/V(III) and V(IV)/V(V) redox pairs existing in the anode and cathode respectively. Finally, in radiochemistry, ^{48}V could be used as a potential imaging or therapeutic isotope; this nuclide is a beta emitter with a 16-day half-life.[19,20] Vanadium is also used as a redox surrogate for neptunium because they have similar redox potentials vs. standard H electrode for the VO_2^+/VO^{2+} and NpO_2^{2+}/NpO_2^+ couples at 1.0 V and 1.15 V respectively.[21]

For several years, we have been investigating the coordination chemistry of isoindoline-based chelates.[22–30] Isoindoline is one of the subunits of phthalocyanine, the aromatic synthetic dye used as a bulk colorant and a specialized material.[31–33] Since the 1950s, isoindoline chelates such as bis(pyridylimino)isoindoline (BPI) have been studied for their metal binding chemistry,[28,34–37] and their metal complexes have been explored for their biomimetic properties,[38,39] as catalysts for organic reactions,[40,41] and for their novel electronic properties.[42,43] However, much of this chemistry has focused on the middle and late transition metal ions; notably, few investigations to date have studied early transition metals. In particular, other than a few reports on its chemistry with molybdenum,[44,45] no examples exist of BPI or other bis(arylimino)isoindoline complexes with metals from groups 3 to 6.

In this article, we present the first study into the vanadium chemistry of a series of chelating isoindoline-based ligands. These compounds, shown in Fig. 1, incorporate pyrazole, indazole, benzimidazole, and pyridine as peripheral heterocycles. All four ligands react rapidly with vanadyl sulfate and vanadyl acetylacetonate to afford 1:1 heteroleptic complexes. The ligands behave as monoanionic, tridentate ligands that bind in a planar geometry. Notably, all products with one exception exhibit vanadium in the +5 oxidation state. Three of the ligands form VO_2 complexes upon reaction with vanadyl sulfate and vanadyl acetylacetonate. The BPI ligand, in contrast, forms a $VO(SO_4)$ complex in the former case and a vanadyl, or V(IV), acetylacetonate in the latter case. All compounds have been fully characterized by X-ray crystallography, spectroscopic methods, and we have

a Department of Chemistry, University of Akron, Akron, Ohio 44325, United States.
b Radioisotope Science and Technology Division, Oak Ridge National Laboratory, 1 Bethel Valley Rd., Oak Ridge, Tennessee 37830, United States.

View Article Online
DOI: 10.1039/D6NJ00601D

elucidated their electronic structures with calculations. These compounds all represent a new class of tridentate, nitrogenous ligand chemistry with vanadium.

Results and discussion

Bis(arylimino)isoindolines were first synthesized in the 1950s by Linstead as part of investigations into the chemistry of isoindoline-based compounds.[32] These tridentate ligands can be readily generated from commercially available reagents in one step, and two methods can be used for their synthesis. Bis(arylimino)isoindolines can be produced by direct reaction of 1,3-diiminoisoindoline with primary amine-modified heterocycles in alcohol solutions[32] or, alternatively, via the reaction of amine-modified heterocycles with phthalonitrile in alcohols in the presence of anhydrous alkaline earth salts.[46] Since their synthesis, bis(arylimino)isoindolines have been shown to avidly bind with a wide variety of transition metal ions and have been used for numerous applications, ranging from biomimetic model complexes to catalysts for organic transformations. However, despite seven decades of research into bis(arylimino)isoindolines and their metal binding chemistry, very little work has focused on the early transition metal chemistry of this class of ligands. To date, only two reports on molybdenum complexes with BPI have been presented,[44,45] and no studies have investigated the chemistry of vanadium.

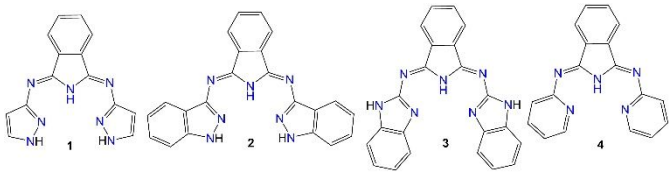

Fig. 1. The structures of the bis(arylimino)isoindoline ligands used in this work.

The structures of the four bis(arylimino)isoindolines are shown in Fig. 1. The four heterocycles that we incorporated into these ligands included pyrazole (**1**), indazole (**2**), benzimidazole (**3**), and pyridine (**4**). All four compounds had been previously synthesized and can be readily produced using the Siegl method with anhydrous $CaCl_2$ as a template and catalyst.[46] Of these four, the structures of compounds **1**, **2**, and **4** were previously elucidated,[22,47] and we were able to determine the structure of compound **3**, which is shown in Fig. S11. The structure of **3** shares many of the attributes present in heterocycle-modified diiminoisoindolines. First, the compounds are all planar with three nitrogen atoms facing the core of the molecule, which is the metal binding site. In all cases, the central isoindoline nitrogen atom is protonated and stabilized by hydrogen bonding interactions with the flanking heterocycle unprotonated nitrogen atom positions. For the three compounds with ionizable heterocycles (**1–3**), the protonated nitrogen positions do not face the central core; in the case of **3**, the ionizable protons reside on the external nitrogen positions. When these ligands bind metal ions, they most typically do so in a meridional fashion, but we observed in our prior work on the chemistry of rhenium that these ligands can be deformed to coordinate in a facial configuration.[28] In the case of the $Re(CO)_3$ complexes, the coordination mode is enforced by the rigid facial configuration of the carbonyl groups.

We reacted ligands **1–4** with two vanadyl starting materials: vanadyl sulfate and vanadyl acetylacetonate. All the reactions afforded crystalline solids that ranged in color from yellow to red-orange, and the chemistry reaction observed for these ligands is shown in Scheme 1. For ligands **1–3**, we observed the formation of the same product using both the vanadyl sulfate and vanadyl acetylacetonate starting material: compounds **$1VO_2$–$3VO_2$** (Fig. 2). The structures of these three compounds are shown in Fig. 3. In each complex, a single equivalent of ligand binds to the vanadium center in a tridentate, planar geometry. The central isoindoline nitrogen atom is deprotonated, resulting in a monoanionic chelate. For **$1VO_2$–$3VO_2$**, the remainder of the vanadium coordination sphere is occupied by two O atoms, which we could assign as oxo groups. The V–O distances range from approximately 1.61 to 1.63 Å, which clearly falls in the V–O double bond range. The V–N bonds range between approximately 2.05 and 2.12 Å, with the central isoindoline V–N bond longer than the flanking V–N bonds. The metals in these complexes exhibit distorted trigonal bipyramidal geometries, with the N–V–N bonds from the flanking heterocycles occupying the axial positions. The axial N–V–N bonds are smaller than the ideal 180° (approximately 150°–165°), and the equatorial O–V–N bonds are, on average, larger than 120° (approximately 125°), with smaller O–V–O angles (approximately 109°). Based on structural features, we could assign the oxidation states in these three complexes as V(V). Additionally, **$1VO_2$–$3VO_2$** exhibited readily interpretable diamagnetic ^1H nuclear magnetic resonance (NMR) spectra.

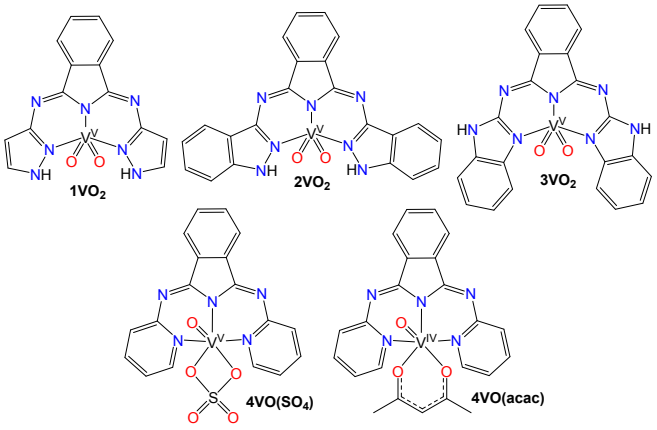

Fig. 2. The structures of the bis(arylimino)isoindoline vanadium complexes

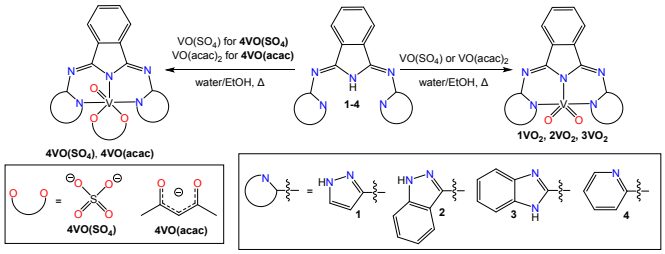

Scheme 1. Synthesis of the bis(arylimino)isoindoline vanadium complexes.

View Article Online
DOI: 10.1039/D6NJ01601D

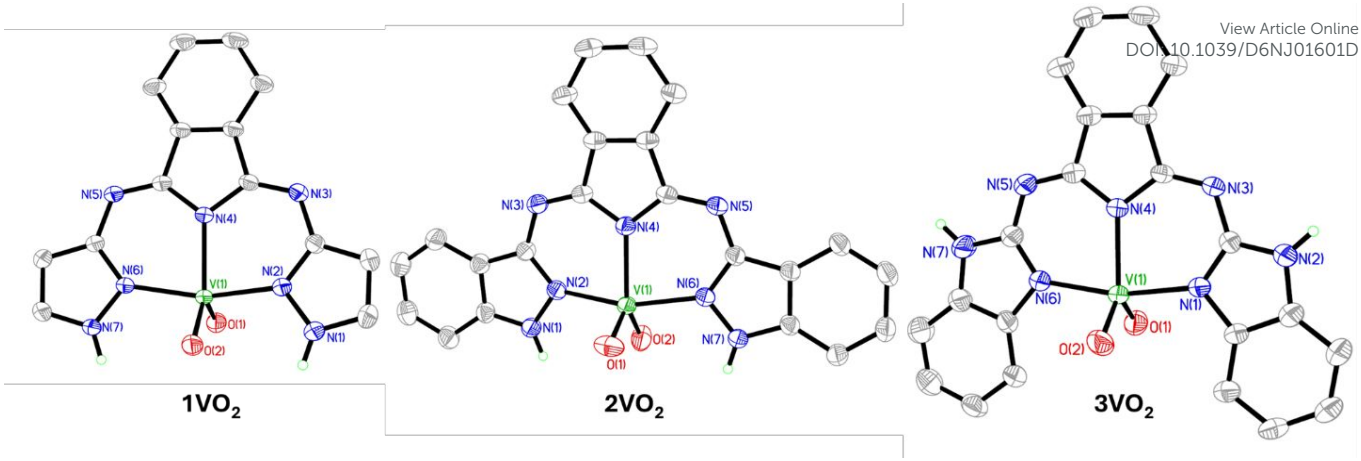

Fig. 3. The structures of compounds **1VO$_2$-3VO$_2$** with 35% thermal ellipsoids. Hydrogen atoms on carbon positions have been omitted for clarity.

For bis(pyridyl) ligand **4**, we observed reactivity dependent on the starting material, which is shown in Scheme 1. When VO(SO$_4$) was employed as the vanadium source, the reaction resulted in a V(V) complex, **4VO(SO$_4$)**, with a sulfate bound at the metal center, as shown on the left side of Fig. 4. In this compound, rather than having a second vanadium oxo bond, a sulfate binds in a bidentate fashion with V–O bond lengths of approximately 1.52 and 1.49 Å. The vanadium oxo bond is slightly shorter than that seen in **1VO$_2$–3VO$_2$**, with a distance of 1.59 Å. BPI binds in a planar tridentate fashion, with the central isoindoline deprotonated, as seen in **1VO$_2$–3VO$_2$**. One notable difference in **4VO(SO$_4$)** is that the V–N bond to the isoindoline nitrogen is shorter (approximately 2.03 Å) than that which is seen with the flanking pyridine groups (approximately 2.13 Å). The diamagnetic character for **4VO(SO$_4$)** was confirmed by ^{1}H NMR spectroscopy, which revealed standard ligand chemical shifts.

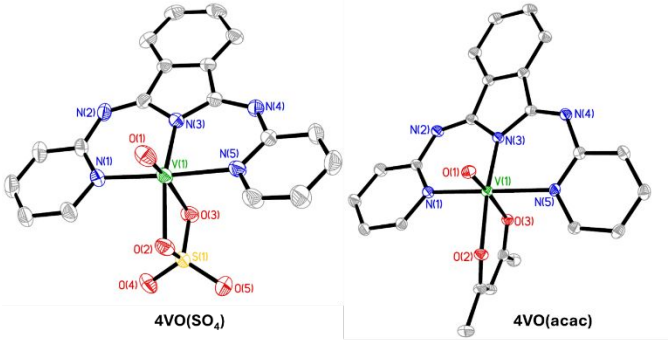

Fig. 4. Structures of (left) **4VO(SO$_4$)** and (right) **4VO(acac)** with 35% thermal ellipsoids. hydrogen atom positions on carbon atoms have been omitted for clarity.

When the BPI chelate reacted with VO(acac)$_2$ as the vanadium source, we observed the formation of a vanadyl complex (**4VO(acac)**), with the metal in the +4 oxidation state. The structure of this lower-valent complex is also shown in Fig. 4. With a monoanionic BPI, a vanadyl unit, and a bidentate acetylacetonate, this compound clearly has V(IV) character. When compared with the similarly structured but higher-valent **4VO(SO$_4$)**, the vanadium oxo bond is slightly longer (approximately 1.61 Å; this may not be chemically significant) but the V–O bonds to the acetylacetonate are much longer than those seen in the sulfate in **4VO(SO$_4$)**, measuring approximately 2.02 and 2.17 Å.

Next, the FTIR spectra of the vanadium complexes were acquired and all V(V) complexes show a band between 961-984 cm^{-1}, attributed to the vanadyl VO$_2$ unit. The V(IV) VO mode in the 4VO(acac) complex is found at 983 cm^{-1}. Additionally, the ligand imine stretching vibration bands are found between 1622-1645 cm^{-1}, these stretches are similarly reported in other bisaryliminoisoindoline ligands.[22] Finally, in the 4VO complexes, the sulfate containing complex portrays S=O stretching at 1062 and 1034 cm^{-1} as well as a SO$_4$ bending vibration at 607 cm^{-1}. The acac complex of 4VO reveals carbonyl stretching bands at 1575 and 1548 cm^{-1} due to the bidentate carbonyl anion.

Spectroscopically, we found evidence that the oxidation state in **4VO(acac)** is V(IV), but we also observed that this complex can be readily oxidized in solution to V(V). In the solid state and in dimethylformamide (DMF) glass at low temperature, **4VO(acac)** exhibited an electron paramagnetic resonance (EPR) spectrum consistent with a V(IV) ion in a rhombic field with hyperfine coupling due to the 7/2 nuclear spin (Fig. S6). In contrast, when **4VO(acac)** was dissolved in dimethyl sulfoxide (DMSO) or CDCl$_3$ in air, we observed diamagnetic chemical shifts in its NMR spectrum. DMSO is slightly oxidizing in potential, so it is not surprising that **4VO(acac)** is oxidized under these conditions.

Surprisingly, only a few meridional nitrogenous ligand complexes of VO$_2$ have been structurally characterized. Several terpyridine complexes of VO$_2$ have been elucidated, but unlike the compounds presented in this report, the (tpy)VO$_2$ compounds are all cationic, with slightly longer V–N bonds than those seen in **1VO$_2$–3VO$_2$**.[48–52] Notably, the central V–N bond is shorter than those seen in the flanking V–N bonds. Most tridentate planar VO$_2$ complexes reported in the literature are anionic and asymmetric. The symmetric anionic complexes include a deprotonated bis(2-pyridylcarbonyl)amine VO$_2$ complex,[53] with V–N bonds of approximately 2.08 Å for the flanking positions and approximately 2.07 Å for the central amide unit, as well as two expanded porphyrin systems, in which the VO$_2$ unit is bound to a tripyrrane segment of the macrocycle.[54,55] In the latter case, the bond lengths vary widely,

View Article Online
DOI: 10.1039/D6NJ01609D

as seen in the flanking V–N bonds that range from approximately 2.08 to 2.15 Å, and may result from macrocyclic steric factors. In the pyrrane compounds, the central V–N bond is the shortest of the three, measuring approximately 2.04 and 2.06 Å in the two compounds. The asymmetric anionic ligand systems belong to two types: aryl-substituted amide with a deprotonated amide N-bound[56] and azole-modified, hydrazine-based ligands.[57] In both types of systems, the V–N bond lengths vary significantly between the different nitrogen donors, but typically, the shortest V–N bond is observed with the formally deprotonated nitrogen position.

We can also compare the vanadium structures of these isoindoline ligands with porphyrin and phthalocyanine vanadyl complexes. In the recently elucidated V(IV) vanadyl etioporphyrin structure, the V-O bond measures ~1.59 Å and the V-N bonds measure approximately 2.07 Å.[58] In vanadyl tetraphenyl porphyrin these bonds are similar in length, ~1.62 and ~2.08 Å respectively.[59] The isoindoline-based phthalocyanine macrocycle has a similar axial V-O bond (~1.58 Å) but appreciably shorter V-N bonds (~2.03 Å), similar to what we observe in our tridentate chelate systems.[60]

All vanadium complexes are colored and strongly absorb in the visible region. The ultraviolet (UV)–visible spectra of the VO_2 and VO complexes are shown in Fig. 5. The spectra of the free base ligands **1–4** are shown in Figs. S7–S10 and exhibit π → π* transitions with a vibronic fine structure.[22] Complexation of the ligands with vanadium resulted in a bathochromic shift in the spectra. In the benzimidazole derivative **3VO₂**, a red-shifted shoulder is shown in the spectrum. Extinction coefficients range between 1.1×10^4 and 2×10^4 M^{-1} cm^{-1} for these compounds.

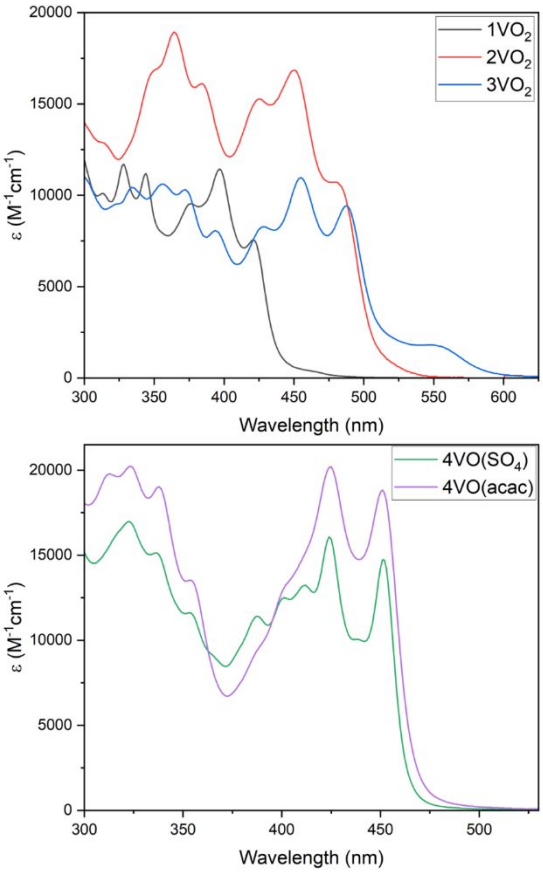

Fig. 5. The UV–visible spectra of the bis(arylimino)isoindoline vanadium complexes in DMF solution. Top spectra show **1VO₂-3VO₂**, and bottom spectra show **4VO(SO₄)** and **4VO(acac)**.

Finally, in order to further understand the electronic structure of the vanadium adducts, we carried out Density Functional Theory (DFT) calculations. The calculated HOMO/LUMO energies and gaps of all vanadium complexes are summarized in Table 1. Complexes **1VO₂–3VO₂** display broadly similar frontier orbital energies, with HOMOs between –6.042 and –5.759 eV and LUMOs clustered near –3.19 to –3.13 eV. Their HOMO–LUMO separations (ΔE_{H-L}) fall in a narrow window (2.57–2.92 eV).

Table 1. DFT (TPPSH(D4)/TZP) calculated HOMO-LUMO energies for all vanadium complexes. Energies are given in eV.

Complex	HOMO	LUMO	ΔE_{H-L}
1VO₂	-6.042	-3.125	-2.917
2VO₂	-5.759	-3.186	-2.573
3VO₂	-5.955	-3.147	-2.808
4VO(SO₄)	-6.326	-5.575	-0.751
4VO(acac)	-5.601	-3.088	-2.513

Within this set, **2VO₂** shows the smallest gap (2.573 eV), mainly due to a higher-lying HOMO (–5.759 eV) compared to **1VO₂** and **3VO₂**, while the LUMOs remain essentially constant across the three. This pattern suggests that substituent- or ligand-dependent effects modulate the donor character (and thus HOMO energy) more strongly than the acceptor manifold (LUMO), which appears largely governed by the vanadium oxo fragment and the conserved coordination environment.

A notably different behavior is observed for **4VO(SO₄)**, which exhibits a dramatically reduced HOMO–LUMO gap (0.751 eV), driven primarily by a much lower LUMO energy (–5.575 eV). This indicates stabilization of low-lying acceptor orbitals relative to the other complexes and implies a substantially altered electronic structure for the sulfate-containing species. In contrast, **4VO(acac)** resembles the **1VO₂–3VO₂** *series more closely* (ΔE_{H-L} = 2.513 eV) possibly due to lower oxidation state of the vanadium, where the pyridine-based isoindoline ligand cannot stabilize the 3d orbitals enough as in **4VO(SO₄)** (Fig. 6). It is noteworthy that looking solely at the HOMO-LUMO gaps will not be able to qualitatively explain the UV-visible spectrum, especially in the case of **4VO(SO₄)**. However, when the gaps between π → π* transitions as shown in Fig. 6., can qualitatively explain the similarities in their absorption spectra.

View Article Online
DOI: 10.1039/D6NJ01601D

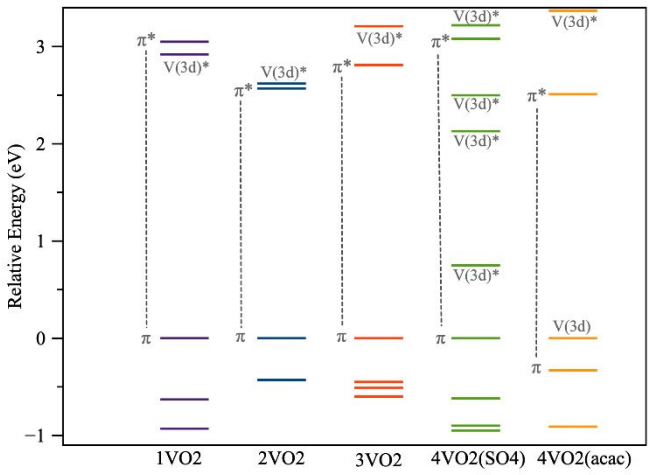

Fig. 6. Energy diagram showing the frontier molecular orbitals relative to the energy of the HOMO of each vanadium complex. Energy gaps shown with dashed lines indicate the $\pi \rightarrow \pi^*$ transitions which do not necessarily correlate with HOMO-LUMO gaps.

Next, the energy decomposition analysis (EDA) results (Table 2) provide insight into the balance of stabilizing and destabilizing contributions governing ligand binding. Across all complexes, the Pauli term is (as expected) strongly destabilizing (+164 to +184 kcal/mol), while the interaction is stabilized by electrostatics (–263 to –296 kcal/mol), orbital interactions (–157 to –200 kcal/mol), and a smaller but non-negligible dispersion term (–8 to –16 kcal/mol). The total interaction energies (ΔE_{int}) follow: ***4VO(SO$_4$)*** *(–327.8 kcal/mol) >* ***1VO$_2$*** *(–309.9 kcal/mol) ≈* ***3VO$_2$*** *(–301.6 kcal/mol) ≈* ***2VO$_2$*** *(–300.4 kcal/mol) >>* ***4VO(acac)*** *(–251.3 kcal/mol).*

Table 2. Energy decomposition analysis on all vanadium complexes from DFT calculations (TPPSH(D4)/TZP). Energies are given in kcal/mol.

Complex	Pauli	Electrostatic	Orbital	Dispersion	Total
1VO$_2$	172.0	-295.9	-177.9	-8.1	-309.9
2VO$_2$	164.1	-279.2	-177.0	-8.4	-300.4
3VO$_2$	163.8	-287.4	-167.8	-10.2	-301.6
4VO(SO$_4$)	166.7	-280.6	-199.9	-14.0	-327.8
4VO(acac)	183.5	-262.6	-156.8	-15.5	-251.3

The three dioxovanadate complexes display closely comparable total interaction energies (–300 to –310 kcal/mol), indicating similar overall metal–ligand binding strengths under the chosen fragmentation. Their stabilization is dominated by a combination of electrostatic attraction (–279 to –296 kcal/mol) and substantial covalent/orbital interaction (–168 to –178 kcal/mol), with dispersion contributing modestly (–8 to –10 kcal/mol). Small variations within the series track primarily with changes in electrostatics and orbital terms rather than dispersion, consistent with subtle electronic tuning by ligand substitution while preserving the same core VO_2^+ bonding framework.

4VO(SO$_4$) shows the most stabilizing total interaction (–327.8 kcal/mol). This also true for the orbital interaction term of the entire set (–199.9 kcal/mol), along with the most stabilizing electrostatic term among the four complexes (–280.6 kcal/mol) and enhanced dispersion (–14.0 kcal/mol). The large orbital contribution points to particularly strong donor–acceptor (covalent) interactions between the isoindoline fragment and the $[VO(SO_4)]^+$ unit in this compound, consistent with a distinct electronic structure relative to the $[VO_2]^+$ -containing complexes. This stronger orbital stabilization is also in line with the unusually low LUMO energy computed for **4VO(SO$_4$)**, i.e., an electronically more accepting fragment. Though this is also complemented by the quasi-linear geometry of the O_{oxo}-V-O_{SO4} which stabilizes through orbital mixing with unoccupied V(V) 3d orbitals as shown in Fig. S16 and Fig. S17. Conversely, and as expected, the lower oxidation state in the **4VO(acac)** complex causes the same isoindoline ligand show lower magnitudes for the attractive forces and a larger Pauli repulsion compared to **4VO(SO$_4$)**. This ultimately causes a lower stabilization of the unoccupied 3d orbitals. The open-shell character of **4VO(acac)** shows the unpaired 3d electron to be the most unstable electron in the system followed by the π-type molecular orbital seen in the other 4 isoindoline complexes.

Conclusions

In conclusion, we synthesized and characterized the first examples of vanadium complexes with isoindoline chelates. These ligands, incorporating pyrazole, indazole, benzimidazole, and pyridine, bind as tridentate planar meridional chelates. In most cases, reacting with vanadyl starting materials results in V(V) compounds, but we did observe a V(IV) species upon metalation of the BPI with vanadyl acetylacetonate. We are currently investigating the electrochemical behavior of these five compounds and will probe their ability to act as catalysts for oxygen transfer reactions and will be reporting on these aspects of their chemistry soon.

General information

Experimental

All reagents and starting materials were purchased from commercial vendors and used without further purification. Deuterated solvents were purchased from Cambridge Isotope Laboratories and used as received. The bis(arylimino)isoindoline ligand precursors **1–4** were prepared using Siegl conditions as previously reported.[22,46]

View Article Online DOI: 10.1039/D6NJ01601D

NMR spectra were recorded on a 400 MHz spectrometer, and chemical shifts were given in parts per million relative to residual solvent resonances (^{1}H NMR spectra). Infrared spectra were collected on a Thermo Scientific Nicolet iS5 that was equipped with an iD5 attenuated total reflectance detector. UV–visible spectra were recorded on a Shimadzu UV-2600 UV–visible spectrometer. Elemental analyses (C, H, N) were performed at Atlantic Microlab on a CHN elemental analyzer. Mass spectroscopy spectra were performed at UTA Research Facilities. EPR spectra were collected on a Bruker X-band ELEXSYS E-500 instrument at 130 K.

X-ray intensity data were measured on a Bruker D8 Venture diffractometer equipped with an Iμs 3.0 Mo X-ray source (λ = 0.71073 Å) and on a Bruker CCD-based diffractometer with dual Cu/Mo IμS microfocus optics (Cu Kα radiation, λ = 1.54178 Å, Mo Kα radiation, λ = 0.71073 Å). APEX4 software was used for data collection and unit cell determination. Crystals were mounted on a cryoloop using Paratone oil and placed under a stream of N_2 at 100 K (Oxford Cryosystems) for **3** and **4VO(acac)** and 300 K for all others. The detector was placed at a distance of 5.00 cm from the crystal. The data were corrected for absorption with the SADABS program. The structures were refined using the Bruker SHELXTL Software Package (Version 6.1)[61] and were solved using direct methods until the final anisotropic full-matrix, least squares refinement of F^2 converged. Disordered solvent in **3VO$_2$** was squeezed out by PLATON.[62]

Computational Details

To further understand the electronic and structural features of the synthesized vanadium complexes, the X-ray crystal structures were used as starting points for a series of geometry optimizations. Initial full optimizations were carried out using the GGA PBE functional with an all-electron TZP basis set, but significant deviations from the experimental metrics were obtained (up to ~9% in V–donor bond lengths for **4VO(SO$_4$)**). Additional optimizations using hybrid (B3LYP and PBE0) and meta-hybrid (TPSSh) functionals were performed to evaluate possible functional dependence. However, the deviations persisted indicating substantial crystal-packing effects not captured by isolated-molecule calculations. Therefore, subsequent calculations employed constrained optimizations in which only hydrogen-atom positions were relaxed, and all non-hydrogen atoms were fixed at their crystallographic coordinates. Single-point energies were then computed at the TPSSh(D4)/TZP level, and energy decomposition analysis (EDA) was performed at the same level of theory. For the EDA, the complexes were partitioned into the corresponding isoindoline ligand fragment and the metal-containing fragment: $[VO_2]^+$ for **1VO$_2$–3VO$_2$**, $[VO(SO4)]^+$ for **4VO(SO$_4$),** and $[VO(acac)]^+$ for **4VO(acac)**. All calculations were performed with the ADF engine within the AMS2025.1 package, including scalar-relativistic effects using the ZORA approximation and implicit solvation (DMF) using COSMO.[63,64]

Syntheses

Syntheses of 1VO$_2$–3VO$_2$. The procedure for generating **1VO$_2$** is representative of these syntheses except that **2** (aryl = indazole, 0.012 g, 0.31 mmol) was used for **2VO$_2$** and **3** (aryl = benzimidazole, 0.12 g, 0.31 mmol) was used for **3VO$_2$**. A solution of **1** (aryl = pyrazole, 0.085 g, 0.31 mmol) was suspended in ethanol (5 mL) in a round bottom flask and heated until all solids went in solution. A solution of $VO(SO_4)$ (0.050 g, 0.31 mmol) was dissolved in 0.5 mL of deionized (DI) water. The aqueous metal solution was added to the hot ethanol solution, and an immediate color change was noted. A precipitate formed in the reaction flask, and the solution was refluxed for 1 h. The solution was cooled to room temperature, filtered, and washed with ethanol. The reaction yielded a yellow-green powder for **1VO$_2$**, orange powder for **2VO$_2$**, and red powder for **3VO$_2$**. Crystals suitable for X-ray diffraction were grown by slow evaporation of DMF.

Syntheses of 4VO(SO$_4$) and 4VO(acac). A solution of **4** (aryl = pyridine, 0.084 g, 0.31 mmol) was suspended in ethanol (5 mL) in a round bottom flask and heated until all solids went into solution. A solution of $VO(SO_4)$ (0.050 g, 0.31 mmol) or $VO(acac)_2$ (0.081 g, 0.31 mmol) was dissolved in 0.5 mL of DI water for $VO(SO_4)$ or ethanol for $VO(acac)_2$. The aqueous metal solution was added to the hot ethanol solution, and an immediate color change was noted. A dark yellow precipitate formed for **4VO(SO$_4$)**, and the solution was refluxed for 1 h. The solution was cooled to room temperature, filtered, and washed with ethanol. The reaction yielding a dark yellow crystalline solid was suitable for X-ray diffraction. No precipitate formed for **4VO(acac)**, and the solution was refluxed for 1 h. The dark yellow solution was cooled to room temperature, and a yellow crystalline solid formed, suitable for X-ray diffraction.

1VO$_2$: Yield: 0.107 g (97%). IR: cm^{-1} 1625 ($\nu_{C=N\ imine}$), 981 ($\nu_{V=O}$). ^{1}H NMR (300 MHz, d6-DMSO): 7.98 (s, 2H), 7.79 (s, 2H), 7.70 (s, 2H), 6.38 (s, 2H). HRMS (ESI-TOF, positive mode) m/z: calcd for $C_{14}H_{11}N_7O_2V$ 360.0414, found 360.0406 $[M+H]^+$.

2VO$_2$: Yield: 0.125 g (82%). IR: cm^{-1} 1622 ($\nu_{C=N\ imine}$), 961 ($\nu_{V=O}$). ^{1}H NMR (300 MHz, d6-DMSO): 13.46 (s, 2H), 8.14–8.12 (m, 4H), 7.76 (s, 2H), 7.58–7.55 (m, 4H), 7.34–7.31 (t, 2H). HRMS (ESI-TOF, positive mode) m/z: calcd for $C_{22}H_{15}N_7O_2V$ 460.0727, found 460.0721 $[M+H]^+$.

3VO$_2$: Yield: 0.052 g (37%). IR: cm^{-1} 1645 ($\nu_{C=N\ imine}$), ($\nu_{V=O}$), 973 ($\nu_{V=O}$). ^{1}H NMR (300 MHz, d6-DMSO): 8.73 (s, 2H), 8.04 (s, 2H), 7.94–7.69 (t, 2H), 7.77 (s, 2H), 7.47–7.44 (d, 2H), 7.29 (m, 2H). *Anal.* Calcd for $C_{22}H_{19}N_7O_{4.5}V$ (**3VO$_2$** + 2.5 H_2O; 504.39): C, 52.39; H, 3.80; N, 19.44. Found: C, 52.38; H, 3.76; N, 19.82.

4VO(SO$_4$): Yield: 0.084 g (65%). IR: 1645 ($\nu_{C=N\ imine}$), 984 ($\nu_{V=O}$), 1062, 1034, 607 (ν_{S-O}). ^{1}H NMR (300 MHz, $CDCl_3$): 8.63–8.62 (d, 2H), 8.13 (s, 2H), 7.80–7.78 (t, 2H), 7.67 (s, 2H), 7.52 (m, 2H), 7.17–7.12 (t, 2H). *Anal.* Calcd for $C_{18}H_{12}N_5O_5SV$ (**4VO(SO$_4$)**; 461.33): C, 46.86; H, 2.62; N, 15.18. Found: C, 47.08; H, 2.79; N, 15.27. HRMS (ESI-TOF, positive mode) m/z: calcd for $C_{19}H_{14}N_5O_3V$ 411.05364, found 411.0528 [M-SO_4+formic acid (FA)]$^+$.

4VO(acac): Yield: 0.071 g (89%). IR: 1635 ($\nu_{C=N\ imine}$), 1575, 1548 ($\nu_{C=O\ AcAc}$), 953 ($\nu_{V=O}$). ^{1}H NMR (300 MHz, $CDCl_3$): 8.63 (s, 2H), 8.09 (s, 2H), 7.79–7.77 (t, 2H), 7.67 (s, 2H), 7.47 (d, 2H), 7.12 (t, 2H), 5.50 (s, H on acac), 2.04 (2, H on acac –CH_3). *Anal.* Calcd for $C_{23}H_{20}N_5O_{3.5}V$ (**4VO(acac)** + 0.5 H_2O; 473.38): C, 58.36; H, 4.26; N, 14.79. Found: C, 58.74; H, 4.18; N, 14.51. HRMS (ESI-TOF,

positive mode) m/z: calcd for $C_{19}H_{14}N_5O_3V$ 411.05364, found 411.0528 [M-acac+formic acid (FA)]$^+$.

Author contributions

The manuscript was written through contributions of all authors. All authors have given approval to the final version of the manuscript.

Conflicts of interest

There are no conflicts to declare.

Data availability

The data supporting this article have been included as part of the Supplementary Information. Spectroscopic data, DFT data, and X-ray parameters. CCDC 2516084-2516089 contains the supplementary crystallographic data for this paper.

Acknowledgements

This material is based upon work supported by the U.S. Department of Energy, Office of Science, Office of Isotope R&D and Production, under contract DE-AC05-00OR22725.

Notes and references

1 L. F. K. Mangini, R. B. G. Valt, M. J. J. de S. Ponte and H. de A. Ponte, *Separation and Purification Technology*, 2020, **246**, 116854.
2 K. Nomura and S. Zhang, *Chemical Reviews*, 2011, **111**, 2342–2362.
3 J.-Q. Wu and Y.-S. Li, *Coordination Chemistry Reviews*, 2011, **255**, 2303–2314.
4 M. Sutradhar, M. A. Andrade, S. A. Carabineiro, L. M. Martins, M. de F. C. Guedes da Silva and A. J. Pombeiro, *Nanomaterials*, 2021, **11**, 1456.
5 R. R. Langeslay, D. M. Kaphan, C. L. Marshall, P. C. Stair, A. P. Sattelberger and M. Delferro, *Chemical reviews*, 2018, **119**, 2128–2191.
6 J. Qian and R. J. Comito, *Organometallics*, 2021, **40**, 1817–1821.
7 D. Rehder, *Journal of inorganic biochemistry*, 2000, **80**, 133–136.
8 R. R. Eady, *Coordination Chemistry Reviews*, 2003, **237**, 23–30.
9 R. Wever, in *Vanadium: biochemical and molecular biological approaches*, Springer, 2011, pp. 95–125.
10 J. M. Winter and B. S. Moore, *Journal of Biological Chemistry*, 2009, **284**, 18577–18581.
11 S. Chattopadhyay, M. K. Chaudhuri and G. C. Mandal, *Journal of Chemical Sciences*.
12 D. Rehder, *Inorganica Chimica Acta*, 2023, **549**, 121387.
13 R. E. Berry, E. M. Armstrong, R. L. Beddoes, D. Collison, S. N. Ertok, M. Helliwell and C. D. Garner, *Angewandte Chemie International Edition*, 1999, **38**, 795–797.
14 Á. Cunha, J. Martins, N. Rodrigues and F. Brito, *International Journal of Energy Research*, DOI:10.1002/er.3260.
15 A. Parasuraman, T. M. Lim, C. Menictas and M. Skyllas-Kazacos, *Electrochimica Acta*, 2013, **101**, 27–40.
16 C. Blanc and A. Rufer, *Paths to Sustainable Energy*, DOI:10.5772/13338.
17 K. Lourenssen, J. Williams, F. Ahmadpour, R. Clemmer and S. Tasnim, *Journal of Energy Storage*, 2019, **25**, 100844–100844.
18 M. U. H. Naseer, B. Pan, S. Wang, Y. Lyu, B. Liu, L. Li, J. Qi and H. Du, *Journal of Environmental Chemical Engineering*, 2025, **13**, 118402.
19 B. A. Broder, M. Bhuiyan, R. Freifelder, D. A. Rotsch, S. K. Chitneni, M. W. Makinen and C.-T. Chen, *Molecules*, 2024, **29**, 799.
20 B. A. Broder, M. P. Bhuiyan, R. Freifelder, H. J. Zhang, A. Kucharski, M. W. Makinen, D. A. Rotsch and C.-T. Chen, *Applied Radiation and Isotopes*, 2022, **186**, 110270.
21 H. B. Andrews and L. R. Sadergaski, *Talanta*, 2023, **259**, 124554.
22 B. R. Schrage, V. N. Nemykin and C. J. Ziegler, *Organic Letters*, 2021, **23**, 1076–1080.
23 C. J. Ziegler, K. Chanawanno, A. Hasheminsasab, Y. V. Zatsikha, E. Maligaspe and V. N. Nemykin, *Inorganic Chemistry*, 2014, **53**, 4751–4755.
24 N. Barone, R. Costa, S. Sripothangnok and C. J. Ziegler, *European Journal of Inorganic Chemistry*, 2010, 775–780.
25 J. T. Engle, G. Martic and C. J. Ziegler, *Makrogeterotsikly*, 2013, **6**, 353–359.
26 S. Gaire, B. R. Schrage, V. N. Nemykin and C. J. Ziegler, *Dalton Transactions*, DOI:10.1039/d0dt04347h.
27 B. R. Schrage, V. N. Nemykin and C. J. Ziegler, *Organic Letters*, 2021, **23**, 5246–5250.
28 B. R. Schrage, D. Vitale, K. A. Kelly, V. N. Nemykin, R. S. Herrick and C. J. Ziegler, *Journal of Organometallic Chemistry*, 2020, **919**, 121331–121331.
29 Y. V. Zatsikha, B. R. Schrage, J. Meyer, V. N. Nemykin and C. J. Ziegler, *Journal of Organic Chemistry*, 2019, **84**, 6217–6222.
30 T. I. Jeaydi, W.-Y. Chen, M. D. Tedesco, B. R. Schrage, V. N. Nemykin and C. J. Ziegler, *RSC Adv.*, 2026, **16**, 24747–24751.
31 R. P. Linstead, *Journal of the Chemical Society (Resumed)*, 1934, 1016–1017.
32 J. A. Elvidge and R. P. Linstead, *Journal of the Chemical Society*, 1952, 5000–5007.
33 P. F. Clark, J. A. Elvidge and R. P. Linstead, *Journal of the Chemical Society*, 1953, 3593–3601.
34 G. Martić, J. T. Engle and C. J. Ziegler, *Inorganic Chemistry Communications*, 2011, **14**, 1749–1752.
35 H. Wen, J. Wang, B. Li, L. Zhang, C. Chen and Z. Chen, *European Journal of Inorganic Chemistry*, 2013, **2013**, 4789–4798.
36 G. Zanotti, F. Palmeri and V. Raglione, *Chemistry–A European Journal*, 2024, **30**, e202400908.
37 V. N. Nemykin and E. A. Lukyanets, *ARKIVOC*, 2010, 136–136.
38 H. Park and D. Lee, *Chemistry–A European Journal*, 2020, **26**, 5916–5926.
39 D. O. Onunga, R. O. Omondi, M. Sitati, G. K. Mutua, D. Jaganyi and A. Mambanda, *Inorganica Chimica Acta*, 2023, **558**, 121730.
40 B. L. Tran, M. Driess and J. F. Hartwig, *Journal of the American Chemical Society*, 2014, **136**, 17292–17301.
41 M. Czaun, J. Kothandaraman, A. Goeppert, B. Yang, S. Greenberg, R. B. May, G. A. Olah and G. K. Surya. Prakash, *ACS Catalysis*, 2016, **6**, 7475–7484.
42 X. Kong, H. Zhao and Y. Tang, *Tetrahedron*, 2023, **144**, 133546.
43 R. Csonka, G. Speier and Jozsef. Kaizer, *RSC Advances*, 2015, **5**, 18401–18419.
44 D. M. Baird, K. Shih, J. Welch and R. D. Bereman, *Polyhedron*, 1989, **8**, 2359–2365.
45 D. M. Baird, R. Hassan and W. Kim, *Inorganica chimica acta*, 1987, **130**, 39–42.

View Article Online
DOI: 10.1039/D6NJ01601D

46 W. O. Siegl, *Journal of Organic Chemistry*, 1977, **42**, 1872–1878.
47 W. Schilf, *Journal of Molecular Structure*, 2004, **691**, 141–148.
48 X.-L. Hong, L.-J. Liu, W.-G. Lu and X.-B. Wang, *Transition Metal Chemistry*, 2017, **42**, 459–467.
49 R. C. Finn and J. Zubieta, *Solid state sciences*, 2002, **4**, 845–849.
50 Y. H. Lee, J. Y. Kim, S. Kusumoto, H. Ohmagari, M. Hasegawa, P. Thuéry, J. Harrowfield, S. Hayami and Y. Kim, *Chemistry*, 2021, **3**, 199–227.
51 M. A. Fik, A. Gorczyński, M. Kubicki, Z. Hnatejko, A. Wadas, P. J. Kulesza, A. Lewińska, M. Giel-Pietraszuk, E. Wyszko and V. Patroniak, *Polyhedron*, 2015, **97**, 83–93.
52 P. J. Hagrman and J. Zubieta, *Inorganic Chemistry*, 2000, **39**, 3252–3260.
53 Z. Azarkamanzad, F. Farzaneh, M. Maghami, J. Simpson and M. Azarkish, *Applied Organometallic Chemistry*, 2018, **32**, e4168.
54 J. L. Sessler, E. Tomat and V. M. Lynch, *Chemical Communications*, 2006, 4486–4488.
55 J. L. Sessler, P. J. Melfi, E. Tomat and V. M. Lynch, *Dalton Transactions*, 2007, 629–632.
56 M. Papanikolaou, S. Hadjithoma, O. Keramidas, C. Drouza, A. Amoiridis, A. Themistokleous, S. C. Hayes, H. N. Miras, P. Lianos and A. C. Tsipis, *Inorganic Chemistry*, 2024, **63**, 3229–3249.
57 M. Ghorbanloo, S. Jafari, R. Bikas, M. S. Krawczyk and T. Lis, *Inorganica Chimica Acta*, 2017, **455**, 15–24.
58 G. L. Pakhomov, A. I. Koptyaev, P. A. Yunin, N. V. Somov, A. S. Semeikin, E. D. Rychikhina and P. A. Stuzhin, *ChemistrySelect*, 2023, **8**, e202303271.
59 M. G. B. Drew, P. C. H. Mitchell and C. E. Scott, *Inorganica Chimica Acta*, 1984, **82**, 63–68.
60 R. F. Ziolo, C. H. Griffiths and J. M. Troup, *J. Chem. Soc., Dalton Trans.*, 1980, 2300–2302.
61 G. M. Sheldrick, *Acta Crystallogr., Sect. A: Found. Crystallogr.*, 2008, **64**, 112–112.
62 A. L. Spek, *Acta Crystallographica Section E*, 2020, **76**, 1–11.
63 E. J. Baerends, N. F. Aguirre, N. D. Austin, J. Autschbach, F. M. Bickelhaupt, R. Bulo, C. Cappelli, A. C. T. van Duin, F. Egidi, C. Fonseca Guerra, A. Förster, M. Franchini, T. P. M. Goumans, T. Heine, M. Hellström, C. R. Jacob, L. Jensen, M. Krykunov, E. van Lenthe, A. Michalak, M. M. Mitoraj, J. Neugebauer, V. P. Nicu, P. Philipsen, H. Ramanantoanina, R. Rüger, G. Schreckenbach, M. Stener, M. Swart, J. M. Thijssen, T. Trnka, L. Visscher, A. Yakovlev and S. van Gisbergen, *The Journal of Chemical Physics*, 2025, **162**, 162501.
64 ADF 2026.1,Theoretical Chemistry SCM, Vrije Universiteit, Amsterdam, The Netherlands,.

View Article Online
DOI: 10.1039/D6NJ01601D

The data supporting this article have been included as part of the Supplementary Information. Spectroscopic data, DFT data, and X-ray parameters. CCDC 2516084-2516089 contains the supplementary crystallographic data for this paper.